



HHS Public Access

Author manuscript

Arterioscler Thromb Vasc Biol. Author manuscript; available in PMC 2023 April 01.

Published in final edited form as:

Arterioscler Thromb Vasc Biol. 2022 April ; 42(4): 381–394. doi:10.1161/ATVBAHA.122.317320.

Intestinal deletion of 3-Hydroxy-3-Methylglutaryl-Coenzyme A Reductase promotes expansion of the resident stem cell compartment

Alexandria M. Doerfler, B.S.^{1,2}, Jun Han, Ph.D.^{3,4}, Kelsey E. Jarrett, Ph.D.^{2,5,6}, Li Tang, Ph.D.^{2,7}, Antrix Jain, M.S.⁸, Alexander Saltzman, Ph.D.⁸, Marco De Giorgi, Ph.D.², Marcel Chuecos, B.S.^{2,9}, Ayrea E. Hurley, B.S.², Ang Li, Ph.D.^{2,10}, Pauline Morand, B.S.¹¹, Claudia Ayala, B.S.², David R. Goodlett, Ph.D.^{3,12}, Anna Malovannaya, Ph.D.^{8,13,14,15}, James F. Martin, M.D., Ph.D.^{1,2,5,9,16,17,18}, Thomas Q. de Aguiar Vallim, Ph.D.^{6,11,19,20}, Noah Shroyer, Ph.D.^{5,9,21}, William R. Lagor, Ph.D.^{1,2,5,9,10,18}

¹Molecular Physiology and Biophysics Graduate Program, Baylor College of Medicine, Houston, Texas, USA.

²Department of Molecular Physiology and Biophysics, Baylor College of Medicine, Houston, Texas, USA.

³University of Victoria - Genome British Columbia Proteomics Centre, Victoria, British Columbia, Canada.

⁴Division of Medical Sciences, University of Victoria, Victoria, British Columbia, Canada.

⁵Integrative Molecular and Biomedical Sciences Graduate Program, Baylor College of Medicine, Houston, Texas, USA.

⁶Department of Medicine, Division of Cardiology, University of California Los Angeles, Los Angeles, USA.

⁷Hunan Provincial Key Lab on Bioinformatics, School of Computer Science and Engineering, Central South University, Changsha 410083, China

⁸Mass Spectrometry Proteomics Core, Baylor College of Medicine, Houston, Texas, USA.

⁹Translational Biology and Molecular Medicine Graduate Program, Baylor College of Medicine, Houston, Texas, USA.

¹⁰Department of Bioengineering, Rice University, Houston, Texas, USA.

¹¹Department of Biological Chemistry, University of California Los Angeles, Los Angeles, USA.

¹²Department of Biochemistry & Microbiology, University of Victoria, Victoria, British Columbia, Canada.

Corresponding author's contact information: William R. Lagor, Ph.D., Molecular Physiology and Biophysics Department, Baylor College of Medicine, Mail stop BCM 335, Houston, TX 77030, Phone: 713-798-8666, lagor@bcm.edu.

Disclosures: J.F.M. is a founder and owns shares in Yap therapeutics. The other authors have no actual or perceived conflicts of interest to disclose.

¹³Verna and Marrs McLean Department of Biochemistry and Molecular Biology, Baylor College of Medicine, Houston, Texas, USA.

¹⁴Department of Molecular and Cellular Biology, Baylor College of Medicine, Houston, Texas, USA.

¹⁵Dan L Duncan Comprehensive Cancer Center, Baylor College of Medicine, Houston, Texas, USA.

¹⁶Cardiomyocyte Renewal Laboratory, Texas Heart Institute, Houston, Texas, USA.

¹⁷Program in Developmental Biology, Baylor College of Medicine, Houston, Texas, USA.

¹⁸Cardiovascular Research Institute, Baylor College of Medicine, Houston, Texas USA.

¹⁹Molecular Biology Institute, University of California Los Angeles, Los Angeles, USA.

²⁰Johnsson Comprehensive Cancer Center, University of California Los Angeles, Los Angeles, USA.

²¹Department of Medicine, Section of Gastroenterology and Hepatology, Baylor College of Medicine, Houston, Texas, USA.

Abstract

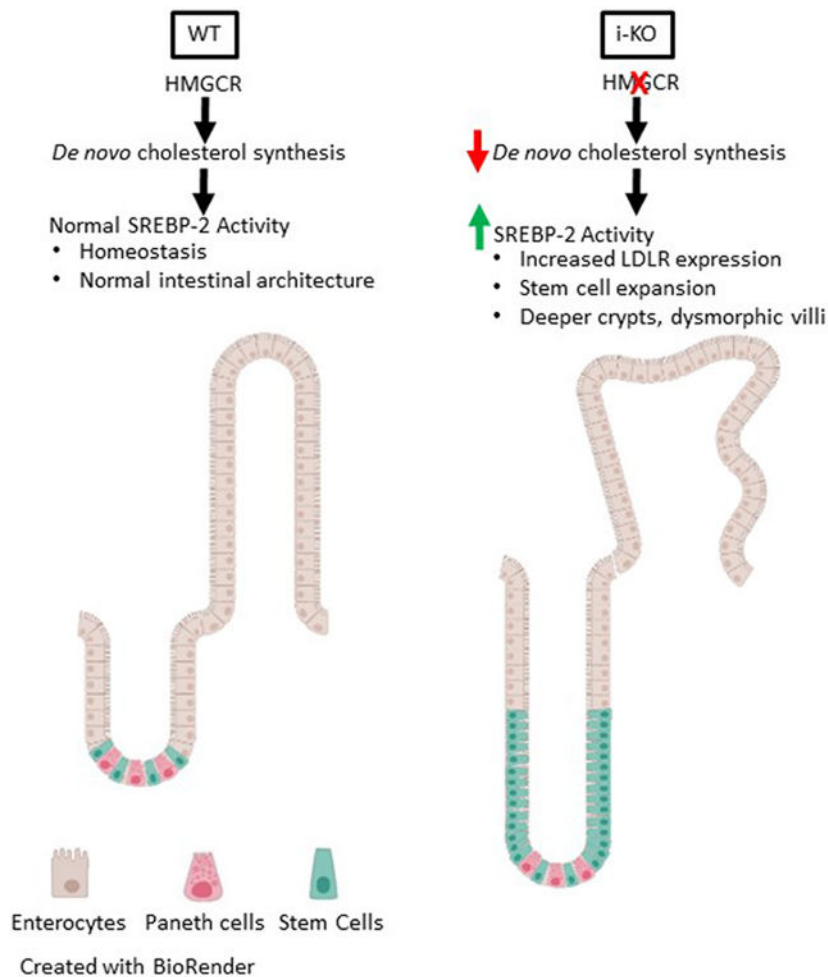
Background: The intestine occupies the critical interface between cholesterol absorption and excretion. Surprisingly little is known about the role of *de novo* cholesterol synthesis in this organ, and its relationship to whole body cholesterol homeostasis. Here we investigate the physiological importance of this pathway through genetic deletion of the rate-limiting enzyme.

Methods: Mice lacking 3-hydroxy-3-methylglutaryl-coenzyme A reductase (*Hmgcr*) in intestinal villus and crypt epithelial cells were generated using a *Villin-Cre* transgene. Plasma lipids, intestinal morphology, mevalonate pathway metabolites, and gene expression were analyzed.

Results: Mice with intestine-specific loss of *Hmgcr* were markedly smaller at birth, but gain weight at a rate similar to wild type littermates, and are viable and fertile into adulthood. Intestine lengths and weights were greater relative to body weight in both male and female *Hmgcr* intestinal knockout (i-KO) mice. Male i-KO had decreased plasma cholesterol levels, while fasting triglycerides were lower in both sexes. Lipidomics revealed substantial reductions in numerous non-sterol isoprenoids and sterol intermediates within the epithelial layer, but cholesterol levels were preserved. *Hmgcr* i-KO mice also showed robust activation of SREBP-2 target genes in the epithelium, including the low-density lipoprotein receptor (LDLR). At the cellular level, loss of *Hmgcr* is compensated for quickly after birth through a dramatic expansion of the stem cell compartment, which persists into adulthood.

Conclusions: Loss of *Hmgcr* in the intestine is compatible with life through compensatory increases in intestinal absorptive surface area, LDLR expression, and expansion of the resident stem cell compartment.

Graphical Abstract



Keywords

Hmgcr; Cholesterol; Absorption of cardiovascular diseases

Subject Terms:

Lipids and Cholesterol; Physiology; Animal Models of Human Disease; Basic Science Research

Introduction

Elevated plasma cholesterol levels are a well-established risk factor for cardiovascular disease¹, and inhibition of cholesterol synthesis with statins remains an essential strategy for cardiovascular disease risk reduction. Statins act by inhibiting 3-hydroxy-3-methylglutaryl-coenzyme A reductase (HMGCR), the rate-limiting enzyme in the mevalonate pathway². The mevalonate pathway is most well-known for the synthesis of cholesterol, but is also responsible for the production of other non-sterol isoprenoids such as farnesyl pyrophosphate (FPP), geranylgeranyl pyrophosphate (GPP), ubiquinone, dolichol, Heme A and Vitamin K². Statins have pleiotropic effects, and depletion of these branch products have

been implicated in their beneficial³⁻⁵ as well as adverse⁶⁻¹¹ events. Cholesterol biosynthesis has been studied in detail in the liver¹², which is the primary target of the statin drugs¹³ and is responsible for the majority of cholesterol clearance from the circulation. However, the importance of the mevalonate pathway in the intestine is largely unexplored. The intestine is of particular interest because it serves as the final mediator of both cholesterol absorption and excretion for the body.

Ohashi *et al.* generated an *Hmgcr* germline knockout mouse (*Hmgcr* KO)¹⁴. Mice with heterozygous loss of *Hmgcr* appeared normal, with preserved rates of cholesterol synthesis in the liver and compensatory upregulation of mevalonate pathway genes. However, homozygous loss of *Hmgcr* is embryonic lethal before embryonic day 8.5 (E8.5), indicating its necessity in early development and implantation¹⁴. Knockout of farnesyl-diphosphate farnesyltransferase 1 (*Fdft1*), which encodes a downstream enzyme that catalyzes the committed step to sterol synthesis, is embryonic lethal around E9.5 with growth retardation and defective neural tube closure^{14,15}. Interestingly, maternally supplied cholesterol could not completely rescue either *Hmgcr* nor *Fdft1* KO models, suggesting that developing embryos are heavily reliant on *de novo* synthesis of non-sterol isoprenoids and cholesterol^{14,15}. Given this critical requirement for the mevalonate pathway in early embryonic development, inducible or tissue-specific knockout models are required to study its role in postnatal physiology. Tissue specific *Hmgcr* KO models have already been generated including liver¹⁶, skeletal muscle¹⁷, adipose tissue¹⁸, myeloid cells¹⁹, pancreatic beta cells²⁰, and T-cells²¹. In nearly all of these examples, loss of *Hmgcr* is detrimental to the viability of the individual target cell type, resulting in severe organ damage and, in some cases, lethality.

Sterol synthesis is regulated through the interaction of three proteins in the endoplasmic reticulum (ER): sterol-regulatory element binding protein-2 (SREBP-2), SREBP-cleavage activating protein (SCAP), and insulin-induced gene (INSIG)². Valuable insight into the importance of the mevalonate pathway in the intestine has been gained through tissue-specific knockouts of *Insig*, *Scap* and *Srebp-2*. McFarlane *et al.* knocked out *Insig1* and *2*, which normally retain SREBPs in the ER²². *Insig1/2* KO mice showed hyper-activation of SREBP-2 and HMGCR, lipidosis of intestinal crypts, and hypercholesterolemia, indicating that the intestine can directly contribute to elevated plasma cholesterol levels when the pathway is overactive²². An inducible *Scap* KO, which is required for escort of both SREBP-1 and 2 to the Golgi, inhibited both fatty acid and cholesterol synthesis, resulting in a severe enteropathy, including collapse of the intestinal mucosa and premature death²³. Organoids cultured from *Scap* KO mice were rescued with oleate and cholesterol supplementation²³, establishing that these lipids are essential for enterocyte viability. Rong *et al.* knocked out *Srebp-2* in the intestine, resulting in enteropathy and impaired survival, which was rescued by dietary cholesterol supplementation²⁴. SREBP-2 is a master regulator of all the genes in the mevalonate pathway including *Hmgcr*, and is a fail-safe mechanism to activate cholesterol synthesis when sterol levels are low. If the lethality observed in the *Srebp-2* intestinal knockout mice is solely due to inhibition of cholesterol synthesis, then deletion of *Hmgcr* in the intestine should not be compatible with life.

In this study, we generated mice with an intestinal-specific knockout of *Hmgcr* using a *Vil1*-Cre transgene. Surprisingly, *Hmgcr* intestinal knockout (i-KO) mice are viable and grow to adulthood. Compensation of early developmental defects in intestinal structure and body weight occurs through increased absorptive surface area, efficient triglyceride absorption, expansion of the stem cell compartment, and upregulation of SREBP-2 target genes- particularly the low-density lipoprotein receptor (LDLR).

Materials and Methods

The data that support the findings of this study are available from the corresponding author upon request. The RNA sequencing data is publicly available on the NCBI Gene Expression Omnibus (GEO) website. The series number is GSE164589, and can be accessed at <https://www.ncbi.nlm.nih.gov/geo/query/acc.cgi?acc=GSE164589>. The targeted proteomics data is publicly available on the MASSIVE website. The series number is PXD026572, and can be accessed at <http://proteomecentral.proteomexchange.org>.

Animals.

Male *C57BL/6J* mice were obtained from The Jackson Laboratory. Mice harboring a “knockout first” allele for *Hmgcr*, *Hmgcr*^{tm1a(KOMP)Wtsi} (*Hmgcr* FRT-FLOX), were generated by the knockout mouse project (KOMP) at the University of California, Davis. These mice were used for generating *Hmgcr* conditional mice harboring exon 5 flanked by loxP sites (*Hmgcr*^{fl/fl})²⁵. Intestine-specific deletion of *Hmgcr* was accomplished by crossing the *Hmgcr*^{fl/fl} mice with B6.Cg-Tg(*Vil1*-cre)1000Gum/J mouse line (JAX stock number 021504). The *Vil1*-Cre *Hmgcr*^{fl/fl} mice were then crossed with the B6.Cg-Gt(ROSA)26Sor^{tm9(CAG-tdTomato)Hze/J} line (JAX stock number 007909) to be used as a reporter for future studies. The “Ai9” tomato reporter in the *Rosa* locus is not known to influence intestinal physiology or lipid metabolism²⁶⁻²⁸, so it was not analyzed as a variable. A list of the complete genotypes of every mouse in each figure is included in the supplemental data excel file. Both male and female mice were used in all experiments unless otherwise stated. Mice were housed in a pathogen-free animal facility with a daylight cycle from 0700 to 1900 hours. Animals were allowed free access to food and water. Mice were maintained on a standard laboratory diet (irradiated PicoLab Select Rodent 50 IF/6F, LabDiet product code 5V5R). To inhibit dietary cholesterol absorption, mice were placed on an ezetimibe diet containing 50 ppm, or 0.005%, ezetimibe (LabDiet 5V5R w/ 50 ppm Ezetimibe, Purple, 5G6K). Non-fasted body weights were measured once weekly, or as otherwise specified, on the weekday of birth beginning at time of weaning. Fasting for lipid measurements was performed for 5 or 16 hours to allow for clearance of intestinally derived triglycerides (TG), as indicated. Plasma was obtained by retro-orbital bleeding with heparinized natelson collecting tubes under the influence of isofluorane anesthesia. For food intake and fecal analyses, mice were singly housed for one week between 4 and 5 weeks of age. All the procedures were performed according to the regulations and with the prior approval of the Institutional Animal Care and Use Committees of the Baylor College of Medicine (protocol AN-6243).

Genotyping.

The *Hmgcr* floxed allele was detected by PCR using primers –5'-AGGGGTAGATGCGTTTCACG-3', 5'-TGAACACGCACTGAAACACC-3'; 400 bp for the floxed allele and 214 bp for the WT allele. Primers to detect the Cre transgene were –5'-ACGACCAAGTGACAGCAATG-3', 5'-CTCGACCAGTTTAGTTACCC-3'; 350 bp. The following primers were used as an internal control: 5'-GAGACTCTGGCTACTCATCC-3', 5'-CCTTCAGCAAGAGCTGGGGAC-3'; 585 bp. Cycling conditions were as follows: 5 min at 95°C followed by 35 cycles of 30 sec at 95°C, 1 min at 60°C, and 1 min at 72°C, then 3 min at 72°C, and holding at 4°C.

DNA Copy Number Analysis.

Intestines were isolated, flushed with PBS, and separated into duodenum, jejunum, and ileum sections based on the method of Casteleyn et al²⁹. Genomic DNA was extracted from duodenal scrapings and 700 ng were subject to digestion with MscI restriction enzyme (NEB). Droplet digital PCR (ddPCR) assays used 50 ng template to amplify the targeted *Hmgcr* region. The *ApoA1* locus was used as a control. A detailed protocol for DNA copy number analysis is available in the data supplement.

RNA analysis.

Intestines were isolated then flushed with PBS, cut open to lay flat, then scraped to collect the epithelial cells from the bottom 2 cm of the duodenum, jejunum, and ileum. RNA isolation was performed using the QIAGEN RNeasy mini kit (Cat. #74106). 500 ng of RNA was reverse transcribed into cDNA using the iScript kit (Cat. #1708891, Bio-Rad). For quantitative PCR (qPCR), the cDNA products were diluted 1:20 into a final reaction volume of 12.5 µl in the wells of a 384-well reaction plate containing 300 nM of each forward and reverse primer, and 6.25 µl of 2X qPCRBIO SyGreen Blue Mix Lo-ROX (Cat. #17-505DB, Genesee Scientific). The following primers were used to amplify exon 5 of mouse *Hmgcr*: forward 5'-TGGGTATTGCTGGCCTCTTC-3', reverse 5'-ACTTTGCTAATGCACTCGCTC-3'. Beta actin was amplified with the following primers: forward 5'-TTGGGTATGGAATCCTGTGG-3', reverse: 5'-CTTCTGCATCCTGTCAGCAA-3'. Relative gene expression was calculated using the Ct method and graphed as fold change relative to beta actin. For RNA sequencing total RNA from 10 liver samples and 10 intestine samples (5 WT and 5 i-KO each) were analyzed by the University of Houston Seq-N-Edit core. A detailed method for RNA sequencing is available in the data supplement.

Plasma Analyses.

Total plasma cholesterol was measured using the Cholesterol E Kit (Cat. #999-02601, Wako Pure Chemical Industries, Ltd.). Total plasma triglycerides were measured using the Infinity triglycerides kit (Cat. #410-00102, ThermoFisher Scientific).

Targeted Lipidomics.

Sterols, isoprenyl phosphates and isoprenoids were extracted from jejunal epithelial scrapings. Sterols were analyzed as previously described with some modifications³⁰.

Lipidomics analyses were conducted at the Genome British Columbia Proteomics Centre, University of Victoria, Canada. A detailed method for targeted lipidomics is available in the data supplement.

Radioactive lipid absorption.

A mixture of 5 μCi ^{14}C -cholesterol, 10 μCi ^3H -triolein, and 2 μg cholesterol were dissolved per ml olive oil as previously described³¹. At 4 weeks of age mice were fasted for 6 hours, then given an oral gavage of the mixture at 15 μl /gram body weight. Immediately after gavage mice were injected intraperitoneally with pluronic-407 (P-407) at a concentration of 37.5 mg/ mL dissolved in PBS (also at 15 μl /gram body weight). Plasma was isolated at 1, 2, 3, and 4 hours post-gavage. At 4 hours post-gavage, mice were euthanized, intestines were isolated and flushed with PBS, and epithelial scrapings were taken from the duodenum, jejunum, and ileum then snap frozen in liquid nitrogen. Plasma (2 μl) was used to count radioactivity with a Beckman Coulter LS 6500 Multi-Purpose Scintillation Counter at each time point. Briefly, counting efficiency of the scintillation counter was determined using the gavage mixture above, and 2 μCi of ^{14}C -cholesterol dissolved in olive oil was used to determine spillover of ^{14}C into the ^3H channel. The counts per million (CPM) given by the scintillation counter were converted to decays per minute (DPM). Total plasma volume was estimated by using the body weight of each mouse³², and this, along with the DPM counted for 2 μl plasma volume, was used to calculate the percent injected dose.

Bile Acid Analysis.

Bile, liver, and intestine were collected from 5-hour fasted mice and were processed as previously described with modifications made to intestinal sample preparation³³. A detailed protocol for bile acid analysis is available in the data supplement.

Immunohistochemistry.

Intestines were flushed with PBS, fixed overnight in 4% PFA at 4°C, dehydrated in 70% EtOH over night at 4°C, then embedded in paraffin using the swiss roll technique³⁴. Immunohistochemistry and hematoxylin and eosin staining were performed by the Texas Medical Center- Digestive Diseases Center, Cellular Morphology core at Baylor College of Medicine. Briefly, sections were deparaffinized and subjected to antigen retrieval with Rodent Decloaker (Cat. #RD913, Biocare). The sections were then incubated with 3% hydrogen peroxide, followed by incubation in normal serum to block nonspecific protein binding. Sections were incubated 1 hour at room temperature with anti-Ki67 (1:75, Cat. #CRM325, Biocare); and anti-Olfm4 (1:500, Cat. #39141S, Cell Signaling). All antibodies were then detected with a Rabbit-on-Rodent HRP-Polymer (Cat. #RMR622H, Biocare) and visualized with DAB chromogen (Cat. #DB801, Biocare). All slides were counterstained with hematoxylin, dehydrated, and mounted with a permanent mounting medium. A Nikon Ci-L bright field microscope was used for imaging at the Integrated Microscopy Core (Baylor College of Medicine). All images quantified were taken at 20X magnification and quantified using ImageJ24 (<https://imagej.nih.gov/ij/>). Detailed methods for crypt and villus area quantification are included in the supplemental methods.

HMGCRC Targeted Proteomics.

Mice were weaned onto a standard laboratory diet at 3 weeks of age, then transitioned to an ezetimibe diet at 6 weeks of age until 12 weeks of age. Jejunal epithelial scrapings were subject to nanoflow LC-MS/MS analysis using a nano-LC 1000 system (Thermo Fisher Scientific, San Jose, CA) coupled to an Orbitrap Fusion (Thermo Fisher Scientific, San Jose, CA) mass spectrometer. A detailed method for HMGCRC targeted proteomics is available in the data supplement.

Western Blot.

Intestines were flushed with PBS then jejunal epithelial scrapings were subject to membrane isolation. 50 μ g of protein were diluted in 4xLDS buffer (Cat# NP0007, Invitrogen) supplemented with 5% β -mercaptoethanol and separated by SDS-PAGE. Proteins were transferred to PVDF membrane and blocked in 5% milk TBS-T (Tween-20, 0.1%). Primary antibodies for LDLR and β -actin were diluted in 5% milk in TBS-T and incubated overnight at 4°C. Secondary antibodies were incubated at room temperature for 1 hour and imaged using an Odyssey Classic (Li-Cor). A detailed method for western blot is available in the data supplement.

Statistical Analysis.

Animal numbers were estimated based on previous experience with each specific assay and expected effect size. No pre-randomization was performed, and researchers were not blind to genotype. Animals were sex and age-matched for all experiments as detailed in the figure legends. Data were tested for normal distribution using the Shapiro-Wilk normality tests. Differences between two groups were assessed with either Welch's t-test for normally distributed data or Mann-Whitney test for non-normally distributed data as detailed in figure legends. Statistical analysis for Mendelian ratios was done using the Binomial test. Statistical analysis for the RNA sequencing was completed as described in the supplemental methods. Statistical analysis for the triglyceride tolerance test was done by performing a Z-test on the area under the curve found for each group. Multiple testing was done for the RNA sequencing analysis using both the Benjamini and Hochberg methods. Corrections for multiple comparisons for the targeted lipidomics and bile acid analysis was completed using the Holm-Šidák method with an $\alpha=0.05$ for adjusted p-value comparisons. P-values < 0.05 were considered statistically significant. All the data are presented as means \pm SD.

Please refer to the Supplemental Materials for detailed protocols, including DNA Copy Number Analysis, RNA sequencing, bile acid analyses, targeted lipidomics targeted proteomics, western blot, triglyceride tolerance test, and intestine barrier function analysis. Additionally, please see the Major Resources Table in the Supplemental Materials.

Results

Hmgcr intestinal knockout mice are viable but markedly smaller at weaning.

Intestinal knockout mice were generated by crossing the conditional *Hmgcr*^{fl/fl} mouse line with the intestine specific B6.Cg-Tg(*Vill*-Cre)^{997Gum/J} mouse line (Figure 1A). The

breeding scheme was designed to maintain the *Vill-Cre* transgene in the hemizygous state (*Vill-Cre*⁺) for all the knockout animals. There were no significant differences in growth curves, histology, or metabolic parameters between the various control genotypes: *Vill-Cre*⁺ *Hmgcr*^{+/+}, *Vill-Cre*⁻ *Hmgcr*^{+/+}, or *Vill-Cre*⁻ *Hmgcr*^{fl/fl} so these were used as controls, and indicated as WT. All genotypes for each mouse used in every figure are included in the supplemental excel file (Supplement Excel_Mouse Genotypes). Intestinal KO mice were viable, although there was a slight deviation from the expected Mendelian ratios based on genotyping at P21 (WT 57.8% vs i-KO 42%, *p* <0.05). (Supplemental Table 1). Successful deletion of *Hmgcr* was confirmed in intestinal epithelial scrapings by ddPCR and qPCR (Figures 1B and 1C, Supplemental Figure S1). Animals with heterozygous deletion of *Hmgcr* in the intestine showed no discernible phenotype consistent with the previously reported germline knockout¹⁴. The most striking feature was that i-KO mice were much smaller than control littermates at time of weaning (3 weeks), and this difference was maintained through 7 weeks of age for females and 12 weeks of age for males (Figures 1A and 1D). Despite efficient knockout of *Hmgcr* in the intestine, no significant differences in plasma cholesterol levels were observed at 5 weeks of age in female mice, although it was significantly lower in male i-KO mice (Figure 1E). In contrast, fasting triglyceride levels were significantly lower in both sexes of i-KO mice (Figure 1F).

Depletion of sterol and non-sterol isoprenoids in the intestinal epithelium.

Targeted lipidomics was performed on intestinal epithelial scrapings from 5-week-old non-fasted male mice to determine the effects of *Hmgcr* deletion on the mevalonate pathway. We were able to detect and quantify a total of 38 metabolites (Supplemental Table S2). There were substantial reductions in the majority of isoprenoid as well as sterol intermediates in the i-KO mice relative to control animals (Figure 2A). This included reduced levels of the branch products Coenzyme Q9 and 10 (CoQ9 and CoQ10), dolichol, and GGPP which are all derived from FPP (Figures 2 B, C). Interestingly the levels of HMG-CoA and mevalonate 5-P did not change reciprocally as would have been expected. This may be due to shunting of these particular metabolites into other pathways or inhibition of their degradation, respectively. Late sterol intermediates indicative of the rates of cholesterol biosynthesis were also markedly reduced- e.g. desmosterol (Figure 2 B, C). The relative abundance of sterol intermediates in the Bloch and Kandutsch-Russell pathways were similarly reduced in i-KO mice, except for 7-dehydrocholesterol (Figures 2 B, C). Collectively, the data indicate a net inhibition of the mevalonate pathway in the intestinal epithelial cells. Notably, cholesterol levels were not reduced in the i-KO mice, even though this end product accounts for the vast majority of carbon flux³⁵.

Compensatory changes in lipid absorption in i-KO mice.

To determine the physiological basis for the smaller size of the i-KO mice, we measured body weights and food intake for singly housed mice between 4 and 5 weeks of age. On the last day of the week, feces were collected in drop-through cages over a 24-hour period. There were no significant differences in overall body weight gained in the 4 to 5 week time span between WT or i-KO mice (Figure 3A). Interestingly, both male and female i-KO mice had higher weeklong food intake when normalized to the starting body weight (Figure 3B). Overall feed efficiencies were similar between i-KO and WT mice (Figure

3C), indicating that there is not an overt defect in nutrient consumption or utilization. The mass of feces excreted as a percent of body weight in 24 hours was similar between both genotypes in males, and slightly larger in female i-KO mice (Figure 3D). We next performed a radiolabeled tracer study to directly assess lipid absorption. i-KO and WT mice were fasted for 6 hours then given an oral gavage of olive oil containing radiolabeled cholesterol and triolein, immediately followed by intraperitoneal injection of P-407 to inhibit lipoprotein lipase activity and triglyceride clearance. Based on the percent-injected dose appearing in the plasma compartment, i-KO mice of both sexes had normal rates of ^{14}C -cholesterol absorption (Figure 3E). Interestingly, the female i-KO mice absorbed more ^3H -triolein than the female WT mice, a trend observed in the male i-KO mice as well (Figure 3F). To understand how the i-KO mice have lower circulating triglycerides but increased triglyceride absorption, mice were fasted 16 hours overnight then injected with a 20% lipid emulsion to bypass gut absorption. Interestingly, the i-KO mice showed no obvious differences in triglyceride excursion (Supplementary Figure S2), possibly due to the longer overnight fast required for this experiment (16 hours vs 5 hours). We then analyzed the total bile acid pool in mice following a five hour fast, to determine if altered quantities or composition of bile acids might be responsible for the increased triglyceride absorption. The total bile acids present in the intestine, liver and gall bladder were not significantly different by genotype, and the total bile acid pool size was unchanged in the i-KO mice (Figure 3G and Supplemental Figure S3). Except for tauro- ω -muricholic acid (T- ω -MCA) in male i-KO mice, the composition of the total bile acid pool remained unchanged, notably including taurocholic acid (TCA) which is a key bile acid promoting lipid absorption^{33,36,37} (Figure 3H, Supplemental Figure S4A-C). At the individual tissue level, T- ω -MCA is decreased in male i-KO mice gall bladder and intestine (Supplemental Figure S4D, S4E, S4I, and S4J). The female i-KO mice show significant decreases in T- α -MCA, taurochenodeoxycholic acid (TCDCa), and tauroolithocholic acid (TLCA) in the bile from the gall bladder (Supplemental Figures S4D, S4F, S4G, and S4H). There were no differences between the WT and i-KO bile acid composition in the liver (Supplemental Figure S4K). The lack of an observed change in TCA levels, paired with the modest decreases observed in other bile acids, makes it unlikely that bile acid composition contributes to increased triglyceride absorption in i-KO mice.

Gene expression changes involving cell division and SREBP-2 target genes.

Given the early embryonic lethality of germline *Hmgcr* KO mice¹⁴, it was surprising that i-KO mice were viable through adulthood and fertile. To gain insight into the underlying biological processes, we examined global gene expression in intestinal epithelial scrapings. RNA from 5 male WT and i-KO mice were subjected to sequencing analysis. A total of 983 genes were upregulated and 714 were downregulated in the intestine based on a $\log_2(\text{foldchange}) > 1.0$ and $p < 0.05$. The most significantly enriched KEGG pathways from the upregulated gene set were: ribosome biogenesis ($p = 2.57^{-18}$), pyrimidine metabolism ($p = 1.6^{-14}$), cell cycle, ($p = 2.57^{-14}$), DNA replication ($p = 1.45^{-12}$), purine metabolism ($p = 1.47^{-10}$), steroid biosynthesis ($p = 2.09^{-08}$), cholesterol biosynthesis ($p = 3.59^{-08}$), and RNA transport ($p = 4.67^{-08}$) (Figure 4A). The most significantly enriched KEGG pathways from the downregulated set were: retinol metabolism ($p = 5.57^{-10}$), drug metabolism – CYP450 ($p = 1.62^{-06}$), arachidonic acid metabolism ($p = 2.12^{-05}$), drug metabolism- other enzymes ($p = 9.22^{-04}$), chemical carcinogenesis ($p = 9.82^{-04}$), metabolism of xenobiotics by

CYP450 ($p=0.0024$), steroid hormone biosynthesis ($p=0.0031$), and glucuronate pathway (urate pathway) ($p=0.0042$) (Figure 4B). This prompted us to consider both cell proliferation as well as upregulation of cholesterol synthesis as potentially important compensatory mechanisms. Since the liver synthesizes the most cholesterol per organ in rodents³⁸, we also analyzed the livers of the same animals. Based on the same parameters as the intestinal epithelial tissue, 411 genes were upregulated in the liver while 146 were down regulated. GO and KEGG pathway analyses showed no significant overlap between pathways upregulated or downregulated in the liver and intestine (Supplemental Figure S5A-C). A detailed examination of the dataset revealed that 14 of the 21 genes in the mevalonate pathway were significantly upregulated in the intestine (Figure 4C); however, there were no corresponding gene expression changes for the mevalonate pathway in i-KO liver tissue (Supplemental Figure S5D). All of these mevalonate pathway genes are known SREBP-2 targets, suggesting hyper-activation of this transcription factor in the intestinal epithelium.

Changes to intestinal architecture and the stem cell compartment following *Hmgcr* deletion.

We postulated that important cellular changes may occur in response to *Hmgcr* deletion based on the enrichment of genes involved in cell division and DNA replication from the RNA sequencing. Therefore, we first examined intestines from the i-KO and WT mice at 5 weeks of age. Histological analysis revealed striking changes to intestinal architecture, including deeper crypts and enlarged, dysmorphic villi (Figure 5A). Quantification of the images showed a doubling in crypt depth (Figure 5B) as well as increased villus area in the jejunum in both male and female i-KO mice (Supplemental Figure S6). At 5 weeks of age i-KO mice had both longer (Figure 5C) and heavier (Figure 5D) intestines than WT littermates relative to body weight. Interestingly, increased intestinal size has been reported in other models of defective intestinal lipid synthesis^{39,40} and intestinal knockouts in the SREBP-2 regulatory network^{23,24}. The *Vill*-Cre transgene is active in villus and crypt epithelial cells of the small and large intestines beginning at E13.5⁴¹. To determine if compensation occurs prior to consumption of solid food, intestines were harvested prior to weaning age at postnatal day 0 (P0), P3, P6, P10, and P21 to measure intestine weights and lengths (Supplemental Figures S7A, S7B). When normalized to body weight, male i-KO mice showed significant increases in intestine weight at P6 and P21, and females show alterations from P6 to P21 (Supplemental Figures S7C). Normalized to body weight, intestine lengths were longer in male i-KO mice at P6, while female i-KO mice show increased intestine length to body weight ratios starting at P21 (Supplemental Figures S7D). H&E staining revealed a disordered and atrophic-looking crypt/villus architecture at P0, consistent with an earlier developmental defect (Figure 5E). Interestingly, the morphology of the intestine is rapidly corrected by P6, where deeper crypts are already noticeable in the i-KO mice (Figure 5F). Staining and quantification for the cellular proliferation marker Ki67 revealed a significant increase in Ki67 expressing cells within the crypts of female i-KO mice by P6 and by P0 in i-KO males (Figures 5G, 5H). The i-KO mice also show a significant increase in the number of stem cells per crypt beginning at P3 based on Olfm4 staining (Figures 5I and 5J). Intestinal stem cell expansion can also alter intestinal barrier function. RNA sequencing showed that Claudin-2 was modestly upregulated in intestinal

epithelial cells, suggesting leaky tight junctions⁴² (Supplemental Figure S8A). To directly assess barrier function, male mice were gavaged with 4-kDa FITC Dextran. We found that the i-KO mice have significantly more FITC Dextran in the plasma as compared to the WT mice, confirming a leakier intestinal barrier (Supplemental Figure S8B).

Maintenance of cholesterol homeostasis upon *Hmgcr* deletion.

The expansion of the stem cell compartment and overall intestinal lengthening should increase demand for cholesterol in the i-KO mice. However, given the magnitude of depletion of the upstream mevalonate-derived intermediates, it appears that synthesis is reduced and cholesterol balance is maintained through other mechanisms- such as increased luminal cholesterol reabsorption or uptake from lipoproteins. To test the requirement for cholesterol reabsorption, male i-KO mice were given a diet containing 0.005% ezetimibe, an inhibitor of the cholesterol transport protein Niemann-Pick C1-Like 1 (NPC1L1), from 6 to 12 weeks of age. Surprisingly, ezetimibe feeding did not adversely affect the health of the mice, as judged by body weights from 6-12 weeks of age (Figure 6A)- in stark contrast to the lethality seen with intestine-specific deletion of *Srebp-2*²⁴. As we saw on standard diet, intestine lengths and weights normalized to body weights were increased in the i-KO mice relative to WT (Figure 6B). Efficient removal of HMGCR levels in excess of 95% was confirmed by targeted LC-MS/MS of 9 different peptides in epithelial scrapings (Figure 6C), confirming that survival is not due to inefficient deletion by Cre recombinase. Interestingly, we observed significantly higher levels of LDLR, a SREBP-2 responsive gene, in agreement with RNA-Seq data (Figure 6D). The increased LDLR protein levels may play an important role in maintaining enterocyte cholesterol levels and viability in these animals, a safeguard that would be absent in the *Srebp-2* intestinal KO mice.

Discussion

HMGCR catalyzes the rate-limiting step in the mevalonate pathway which produces both cholesterol and non-sterol isoprenoids that are required for the growth of all mammalian cells. Given the importance of HMGCR in early embryonic development¹⁴, as well as cellular viability *in vitro*³⁵, it is quite surprising that tissue-specific loss of this gene in the intestine is compatible with life. This is also interesting given the severe phenotypes seen in knockouts of key regulators of the pathway, such as *Scap* and *Srebp-2*^{23,24}, which act upstream of *Hmgcr* to drive *de novo* synthesis of cholesterol. Here we report that *Hmgcr* i-KO mice are viable and fertile into adulthood. These animals show a regenerative phenotype in the intestine, characterized by a dramatic expansion of the resident stem cell compartment. Although initially smaller, *Hmgcr* i-KO mice have preserved lipid absorption and longer intestines, allowing them to gain weight at a rate similar to wild type littermates. Cholesterol mass in the intestinal epithelium is maintained in the absence of HMGCR, suggesting plasticity in sourcing this critical metabolite from luminal reabsorption or lipoprotein uptake.

We initially suspected that *Hmgcr* deletion by the *Vill*-Cre transgene, although it starts at E13.5⁴¹, might be incomplete. Cells in the crypt that escape complete *Hmgcr* deletion could then have a selective advantage, allowing them to clonally expand and regenerate

the villi with HMGCR⁺ epithelial cells. However, we observed highly efficient deletion in epithelial scrapings by ddPCR for exon 5, qPCR for *Hmgcr* mRNA, and targeted LC-MS/MS for peptides from the HMGCR protein. In addition, we found robust decreases in mevalonate-derived intermediates in epithelial scrapings from these animals. This indicates that at any given point in time, the vast majority (>95%) of intestinal epithelial cells are HMGCR-deficient. Even if there is a small pool of HMGCR⁺ stem cells in the crypt, their descendants have a sufficient supply of sterols and non-sterol isoprenoids to survive, differentiate, and migrate up the villus- in spite of ongoing Cre activity. Taken together, this means HMGCR activity is not absolutely required for viability within the short lifetime of an intestinal epithelial cell.

The initially smaller size of *Hmgcr* i-KO mice suggests a defect in nutrient absorption. We attempted to assess the physiological impact of HMGCR loss on feeding behavior, feed efficiency, and lipid absorption at 4-5 weeks of age. Overall, we saw increased food intake and similar or increased rates of triglyceride absorption. This translated to body weight gain that was similar to wild type, which was remarkable given the efficiency of *Hmgcr* deletion. To better understand the basis for preserved lipid absorption, we performed a comprehensive survey of bile acids in the liver, gall bladder, and intestines of these animals. While some minor differences in composition were observed, *Hmgcr* i-KO mice had a bile acid pool size that was indistinguishable from wild type littermates. Therefore, the most plausible explanation for the preserved lipid absorption and growth rates in these animals appears to be the longer and heavier intestines, which would provide greater absorptive capacity relative to the size of the animals. Longer and heavier intestines also showed important histological differences including deeper crypts and dysmorphic villi, indicative of a regenerative phenotype. Early in the postnatal period, *Hmgcr* i-KO mice already showed dramatic increases in crypt depth, proliferating Ki67⁺ cells, and Olfm4⁺ stem cells. The approximate doubling of crypt depth and stem cell expansion is maintained into adulthood, consistent with a recurring intestinal injury and ongoing compensation.

Targeted lipidomics showed that numerous isoprenoids and intermediates were dramatically reduced in the *Hmgcr* i-KO mice, but cholesterol levels were not changed. This is remarkable, especially given that late sterol intermediates are regarded as excellent surrogates for the rate of *de novo* synthesis. This indicates that the epithelial cells are obtaining cholesterol from other sources, such as reabsorption of biliary cholesterol from the lumen or uptake from circulating lipoproteins. We did not observe any substantial changes to the bile acid pool or composition that could explain increased cholesterol uptake. Likewise, *Npc1l1* mRNA expression was lower in the *Hmgcr* i-KO mice (data not shown), also arguing against increased biliary cholesterol reabsorption. Therefore we placed mice on a diet containing 0.005% ezetimibe to directly inhibit cholesterol absorption⁴³. Surprisingly, this had no appreciable effect on body weight gain or health of the animals, in direct contrast to cholesterol auxotrophy seen with intestinal deletion of *Srebp-2*²⁴. Western blotting showed significantly higher LDLR levels in the *Hmgcr* i-KO mice relative to control animals, consistent with hyperactivation of SREBP-2 target genes seen by RNA-Seq. These data suggest that LDLR-mediated uptake from circulating lipoproteins may become an important source of cholesterol for enterocytes lacking the ability to synthesize it.

The viability of the i-KO mice we have generated is in direct contrast with mice lacking SREBP-2, a master regulator of the mevalonate pathway²⁴. This is paradoxical, since SREBP-2 activates transcription of *Hmgcr* when sterol levels are low and there should still be some level of residual HMGCR activity in that situation. Perhaps the lethality seen with intestinal deletion of *Srebp-2* is due to an inability to upregulate LDLR- a critical safeguard that is preserved in the *Hmgcr* i-KO mice. It is also possible that the lethality observed in intestinal *Srebp-2* KO mice could involve non-canonical roles for this transcription factor. In fact, there are data indicating roles for SREBP-2 in unexpected processes in the gut, including regulation of gut peptide secretion through the expression of bitter taste receptors⁴⁴. SREBP-2 has also been implicated in stem cell self-renewal in zebrafish through Notch signaling⁴⁵. This may be a critical function that is lost in the *Srebp-2* intestinal KO mice, but preserved or even enhanced in the *Hmgcr* i-KO mice. In support of this possibility, Wang *et al.* showed that loss of the phospholipid remodeling enzyme Lysophosphatidylcholine Acyltransferase 3 (*Lpcat3*), in the intestine stimulates cholesterol biosynthesis, leading to stem cell proliferation and increased tumorigenesis⁴⁶. This effect was ascribed to increased cholesterol synthesis, based on potent transcriptional upregulation of the mevalonate pathway, similar to what we have observed. However, in our model there is a marked reduction in the mevalonate derived metabolites and late sterol intermediates, strongly suggesting net decreased synthesis. Perhaps the crypt expansion seen in both the *Hmgcr* i-KO mice and the *Lpcat3* KO mice is actually due to activation of an SREBP-2-driven stem cell expansion program. This is an intriguing possibility that merits further study.

In summary, we have shown that intestinal loss of *Hmgcr* is compatible with life, and mice lacking this critical enzyme survive into adulthood and are fertile. The immediate impact appears to be a developmental defect in intestinal architecture that is evident at birth along with reduced body weights at weaning. Interestingly, the i-KO mice compensate for the lack of *Hmgcr* through intestinal stem cell proliferation in the crypts, as well as upregulation of SREBP-2 targets, including LDLR. The net effect of these compensatory changes are mice with heavier and longer intestines relative to body weight and that have preserved capacity for lipid absorption. This will be a valuable model to investigate the necessity of cholesterol and other non-sterol isoprenoids in intestinal stem cell biology, and should provide valuable new insights into intestinal stem cell function and lipid metabolism.

Supplementary Material

Refer to Web version on PubMed Central for supplementary material.

Acknowledgments

The University of Victoria-Genome BC Proteomics Center is grateful to Genome Canada, Genome Alberta and Genome British Columbia for financial support for Genomics Technology Platforms (GTP) funding for operations and technology development (MC4 and 265MET), and to the Canada Foundation for Innovation, through the Major Science Initiatives Fund (CFI-MSI). The authors also wish to acknowledge Drs. Yinghong Pan and Brandon Mistretta at the University of Houston Seq-N-Edit Core for performing the RNA sequencing.

Sources of Funding

This research was supported by NIH grants (HL132840 and DK124477 to W.R.L., HL127717, HL130804, and HL118761 to J.F.M., and DK128952 and DK118064 to T.Q.d.A.V.), Vivian L. Smith Foundation (J.F.M.), State of Texas funding (J.F.M.), Foundation LeDucq Transatlantic Networks of Excellence in Cardiovascular Research (14CVD01) 'Defining the genomic topology of atrial fibrillation' (J.F.M.), American Heart Association fellowships (19PRE34380467 to A.M.D. and 19POST34430092 to M.D.G.), and T32 training grants (T32HL07676 to A.M.D. and K.E.J., and T32GM08321 and T32HL069766 to K.E.J.). This work was also supported by the Texas Digestive Diseases Morphology Core (P30DK56338), the Baylor College of Medicine Integrated Microscopy Core (DK56338, and CA125123), and the Columbia University Irving Institute for Clinical and Translational Research Biomarkers Core Facility at the (UL1-TR-001873). BCM Mass Spectrometry Proteomics Core is supported by the Dan L. Duncan Comprehensive Cancer Center NIH award (P30 CA125123) and CPRIT Core Facility Award (RP170005 and RP210227).

Abbreviations:

HMGCR	3-hydroxy-3-methylglutaryl coenzyme A reductase
FPP	farnesyl pyrophosphate
GPP	geranylgeranyl pyrophosphate
KO	knockout
ER	endoplasmic reticulum
SREBP	sterol-regulatory element binding protein
SCAP	SREBP-cleavage activating protein
Insig	insulin-induced gene
LDLR	low-density-lipoprotein receptor
ddPCR	droplet digital polymerase chain reaction
GO	gene ontology
KEGG	Kyoto Encyclopedia of Genes and Genomes
HDCA	Hyodeoxycholic acid
TLCA	Taurolithocholic acid
TDCA	Taurodeoxycholic acid
TCA	Taurocholic acid
TCDC	Taurochenodeoxycholic acid
DCA	Deoxycholic acid
CA	Cholic acid
CDCA	Chenodeoxycholic acid
T-ω-MCA	Tauro- ω -muricholic acid
T-β-MCA	Tauro- β -muricholic acid

T-α-MCA	Tauro- α -muricholic acid
β-MCA	β -muricholic acid
α-MCA	α -muricholic acid
NPC1L1	Niemann-Pick C1-Like 1
LPCAT3	Lysophosphatidylcholine Acyltransferase 3

References

1. Virani SS, Alonso A, Benjamin EJ, Bittencourt MS, Callaway CW, Carson AP, Chamberlain AM, Chang AR, Cheng S, Delling FN, et al. Heart disease and stroke statistics—2020 update: A report from the American Heart Association.; 2020.
2. Brown MS, Goldstein JL. Cholesterol feedback: from Schoenheimer's bottle to Scap's MELADL. *The Journal of Lipid Research*. 2008;50(Supplement):S15–S27. [PubMed: 18974038]
3. Oesterle A, Laufs U, Liao JK. Pleiotropic Effects of Statins on the Cardiovascular System. *Circulation Research*. 2017;120(1):229–243. [PubMed: 28057795]
4. Buhaescu I, Izzedine H. Mevalonate pathway: A review of clinical and therapeutical implications. *Clinical Biochemistry*. 2007;40(9–10):575–584. [PubMed: 17467679]
5. Ridgway ND, McLeod RS. *Biochemistry of Lipids, Lipoproteins and Membranes.*; 2016.
6. Jacobson TA. NLA Task Force on Statin Safety--2014 update. *Journal of clinical lipidology*. 2014;8(3 Suppl):S1–4.
7. Nikolic D, Banach M, Chianetta R, Luzzu LM, Stoian AP, Diaconu CC, Citarrella R, Rizzo M, Nikolic D, Banach M, et al. Expert Opinion on Drug Safety An overview of statin-induced myopathy and perspectives for the future. *Expert Opinion on Drug Safety*. 2020;00(00):1–15.
8. Crandall JP, Mather K, Rajpathak SN, Goldberg RB, Watson K, Foo S, Ratner R, Barrett-Connor E, Temprosa M. Statin use and risk of developing diabetes: Results from the diabetes prevention program. *BMJ Open Diabetes Research and Care*. 2017.
9. Brault M, Ray J, Gomez YH, Mantzoros CS, Daskalopoulou SS. Statin treatment and new-onset diabetes: A review of proposed mechanisms. *Metabolism: Clinical and Experimental*. 2014;63(6):735–745. [PubMed: 24641882]
10. Anon. LiverTox: Clinical and Research Information on Drug-Induced Liver Injury [Internet]. National Institute of Diabetes and Digestive and Kidney Diseases. 2017;(August).
11. Meurer L, Cohen SM. Drug-Induced Liver Injury from Statins. *Clinics in Liver Disease*. 2020;24(1):107–119. [PubMed: 31753243]
12. Trapani L, Segatto M, Pallottini V. Regulation and deregulation of cholesterol homeostasis: The liver as a metabolic “power station.” *World Journal of Hepatology*. 2012;4(6):184–190. [PubMed: 22761969]
13. Istvan ES, Deisenhofer J. Structural mechanism for statin inhibition of HMG-CoA reductase. *Science*. 2001;292(5519):1160–1164. [PubMed: 11349148]
14. Ohashi K, Osuga JI, Tozawa R, Kitamine T, Yagyu H, Sekiya M, Tomita S, Okazaki H, Tamura Y, Yahagi N, et al. Early Embryonic Lethality Caused by Targeted Disruption of the 3-Hydroxy-3-methylglutaryl-CoA Reductase Gene. *Journal of Biological Chemistry*. 2003;278(44):42936–42941.
15. Tozawa RI, Ishibashi S, Osuga JI, Yagyu H, Oka T, Chen Z, Ohashi K, Perrey S, Shionoiri F, Yahagi N, et al. Embryonic lethality and defective neural tube closure in mice lacking squalene synthase. *Journal of Biological Chemistry*. 1999;274(43):30843–30848.
16. Nagashima S, Yagyu H, Ohashi K, Tazoe F, Takahashi M, Ohshiro T, Bayasgalan T, Okada K, Sekiya M, Osuga JI, et al. Liver-specific deletion of 3-hydroxy-3-methylglutaryl coenzyme a reductase causes hepatic steatosis and death. *Arteriosclerosis, Thrombosis, and Vascular Biology*. 2012;32(8):1824–1831.

17. Osaki Y, Nakagawa Y, Miyahara S, Iwasaki H, Ishii A, Matsuzaka T, Kobayashi K, Yatoh S, Takahashi A, Yahagi N, et al. Skeletal muscle-specific HMG-CoA reductase knockout mice exhibit rhabdomyolysis: A model for statin-induced myopathy. *Biochemical and Biophysical Research Communications*. 2015;466(3):536–540. [PubMed: 26381177]
18. Yeh Y, Jheng H, Iwase M, Nomura W, Yeh Y, Jheng H, Iwase M, Kim M, Mohri S, Kwon J, et al. The Mevalonate Pathway Is Indispensable for Adipocyte Survival. *ISCIENCE*. 2018;9:175–191. [PubMed: 30396151]
19. Sakai K, Nagashima S, Wakabayashi T, Tumenbayar B, Hayakawa H, Hayakawa M, Karasawa T, Ohashi K, Yamazaki H, Takei A, et al. Myeloid hmg-coa (3-hydroxy-3-methylglutaryl-coenzyme a) reductase determines atherosclerosis by modulating migration of macrophages. *Arteriosclerosis, Thrombosis, and Vascular Biology*. 2018;38(11):2590–2600.
20. Takei S, Nagashima S, Takei A, Yamamuro D, Wakabayashi T, Murakami A, Isoda M, Yamazaki H, Ebihara C, Takahashi M, et al. β Cell-Specific Deletion of HMG-CoA (3-hydroxy-3-methylglutaryl-coenzyme A) Reductase Causes Overt Diabetes Due to Reduction of β Cell Mass and Impaired Insulin Secretion. *Diabetes*. 2020;db190996.
21. Lacher SM, Bruttger J, Kalt B, Berthelet J, Rajalingam K, Wörtge S, Waisman A. HMG-CoA reductase promotes protein prenylation and therefore is indispensable for T-cell survival. *Cell Death and Disease*. 2017;8(5):e2824. [PubMed: 28542128]
22. McFarlane MR, Liang G, Engelking LJ. Insig proteins mediate feedback inhibition of cholesterol synthesis in the intestine. *Journal of Biological Chemistry*. 2014;289(4):2148–2156.
23. McFarlane MR, Cantoria MJ, Linden AG, January B a., Liang G, Engelking LJ. Scap is required for sterol synthesis and crypt growth in intestinal mucosa. *Journal of Lipid Research*. 2015;56(8):1560–1571. [PubMed: 25896350]
24. Rong S, McDonald JG, Engelking LJ. Cholesterol auxotrophy and intolerance to ezetimibe in mice with SREBP-2 deficiency in the intestine. *Journal of Lipid Research* . 2017;58(10):1988–1998. [PubMed: 28630260]
25. De Giorgi M, Jarrett KE, Burton JC, Doerfler AM, Hurley A, Li A, Hsu RH, Furgurson M, Patel KR, Han J, et al. Depletion of essential isoprenoids and ER stress induction following acute liver-specific deletion of HMG-CoA Reductase. *Journal of Lipid Research*. 2020;jlr.RA120001006.
26. Madisen L, Zwingman TA, Sunkin SM, Oh SW, Zariwala HA, Gu H, Ng LL, Palmiter RD, Hawrylycz MJ, Jones AR, et al. A robust and high-throughput Cre reporting and characterization system for the whole mouse brain. *Nature Neuroscience*. 2010;13(1):133–140. [PubMed: 20023653]
27. Wang M, Sun Z, Zou Z, Ding F, Li L, Wang H, Zhao C, Li N, Dai Y. Efficient targeted integration into the bovine Rosa26 locus using TALENs. *Scientific Reports*. 2018;8(1):1–10. [PubMed: 29311619]
28. Perez-Pinera P, Ousterout DG, Brown MT, Gersbach CA. Gene targeting to the ROSA26 locus directed by engineered zinc finger nucleases. *Nucleic Acids Research*. 2012;40(8):3741–3752. [PubMed: 22169954]
29. Casteleyn C, Rekecki A, Van Der Aa A, Simoens P, Van Den Broeck W. Surface area assessment of the murine intestinal tract as a prerequisite for oral dose translation from mouse to man. *Laboratory Animals*. 2010;44(3):176–183. [PubMed: 20007641]
30. Tang Z, Guengerich FP. Dansylation of unactivated alcohols for improved mass spectral sensitivity and application to analysis of cytochrome P450 oxidation products in tissue extracts. *Anal Chem*. 2010;81(18):77006–7712.
31. Bietrix F, Yan D, Nauze M, Rolland C, Bertrand-michel J, Come C, Schaak S, Barbaras R, Groen AK, Perret B, et al. Accelerated Lipid Absorption in Mice Overexpressing Intestinal SR-BI. 2006;281(11):7214–7219.
32. Riches AC, Sharp JG, Thomas DB, Smith SV. Blood Volume Determination in the Mouse. *Journal of Physiology*. 1973:279–284.
33. Clifford BL, Sedgeman LR, Williams KJ, Morand P, Cheng A, Jarrett KE, Chan AP, Brearley-Sholto MC, Wahlström A, Ashby JW, et al. FXR activation protects against NAFLD via bile-acid-dependent reductions in lipid absorption. *Cell Metabolism*. 2021;33(8):1671–1684.e4. [PubMed: 34270928]

34. Bialkowska AB, Ghaleb AM, Nandan MO, Yang VW. Improved Swiss-rolling Technique for Intestinal Tissue Preparation for Immunohistochemical and Immunofluorescent Analyses. 2016; (July):1–8.
35. Faust JR, Luskey KL, Chin DJ, Goldstein JL, Brown MS. Regulation of synthesis and degradation of 3-hydroxy-3-methylglutaryl-coenzyme A reductase by low density lipoprotein and 25-hydroxycholesterol in UT-1 cells. Proceedings of the National Academy of Sciences of the United States of America. 1982;79(17):5205–5209. [PubMed: 6957860]
36. Li-Hawkins J, Gåfvæls M, Olin M, Lund EG, Andersson U, Schuster G, Björkhem I, Russell DW, Eggertsen G. Cholic acid mediates negative feedback regulation of bile acid synthesis in mice. Journal of Clinical Investigation. 2002;110(8):1191–1200.
37. Bertaggia E, Jensen KK, Castro-Perez J, Xu Y, Paolo G Di, Chan RB, Wang L, Haeusler RA. Cyp8b1 ablation prevents Western diet-induced weight gain and hepatic steatosis because of impaired fat absorption. American Journal of Physiology - Endocrinology and Metabolism. 2017;313(2):E121–E133. [PubMed: 28377401]
38. Spady DK, Dietschy JM. Sterol synthesis in vivo in 18 tissues of the squirrel monkey, guinea pig, rabbit, hamster, and rat. Journal of lipid research. 1983;24(3):303–315. [PubMed: 6842086]
39. Rong X, Wang B, Dunham MM, Hedde PN, Iklas W, Wong JS, Gratton E, Young SG, Ford DA, Tontonoz P. Lpcat3-dependent production of arachidonoyl phospholipids is a key determinant of triglyceride secretion. eLife. 2015;4:1–23.
40. Zhang P, Csaki LS, Ronquillo E, Baufeld LJ, Lin JY, Gutierrez A, Dwyer JR, Brindley DN, Fong LG, Tontonoz P, et al. Lipin 2/3 phosphatidic acid phosphatases maintain phospholipid homeostasis to regulate chylomicron synthesis. Journal of Clinical Investigation. 2018;129(1):281–295.
41. Madison BB, Dunbar L, Qiao XT, Braunstein K, Braunstein E, Gumucio DL. Cis Elements of the Villin Gene Control Expression in Restricted Domains of the Vertical (Crypt) and Horizontal (Duodenum, Cecum) Axes of the Intestine. Journal of Biological Chemistry. 2002;277(36):33275–33283.
42. Zeissig S, Bürgel N, Günzel D, Richter J, Mankertz J, Wahnschaffe U, Kroesen AJ, Zeitz M, Fromm M, Schulzke JD. Changes in expression and distribution of claudin 2, 5 and 8 lead to discontinuous tight junctions and barrier dysfunction in active Crohn's disease. Gut. 2007;56(1):61–72. [PubMed: 16822808]
43. Engelking LJ, McFarlane MR, Li CK, Liang G. Blockade of cholesterol absorption by ezetimibe reveals a complex homeostatic network in enterocytes. Journal of Lipid Research. 2012;53(7):1359–1368. [PubMed: 22523394]
44. Jeon T II, Zhu B, Larson JL, Osborne TF. SREBP-2 regulates gut peptide secretion through intestinal bitter taste receptor signaling in mice. Journal of Clinical Investigation. 2008;118(11):3693–3700.
45. Gu Q, Gu Q, Yang X, Lv J, Zhang J, Xia B, Kim J, Wang R, Xiong F, Miller YI, et al. AIBP-mediated cholesterol efflux instructs hematopoietic stem and progenitor cell fate. Science. 2019;1749(March):eaav1749.
46. Wang B, Rong X, Palladino E, Wang J, Fogelman A, Martin M, Alrefai W, Ford D, Tontonoz P. Phospholipid remodeling and cholesterol availability regulate intestinal stemness and tumorigenesis. Cell Stem Cell. 2018;22(2):206–220. [PubMed: 29395055]
47. De Giorgi M et al. Targeting the ApoA1 locus for liver-directed gene therapy. Mol. Ther. Methods Clin. Dev 21, 656–669 (2021). [PubMed: 34141821]
48. Conesa A et al. A survey of best practices for RNA-seq data analysis. Genome Biol. 17, 1–19 (2016). [PubMed: 26753840]

Highlights:

- Mice lacking Hmgcr in the intestine are born smaller than controls, but are viable and fertile.
- Compensatory changes preserve lipid absorption through increased intestinal surface area.
- SREBP-2 target genes are significantly upregulated in the Hmgcr i-KO mice, including LDLR.
- Hmgcr i-KO intestines show increased proliferation and a dramatic expansion of the resident stem cell compartment.

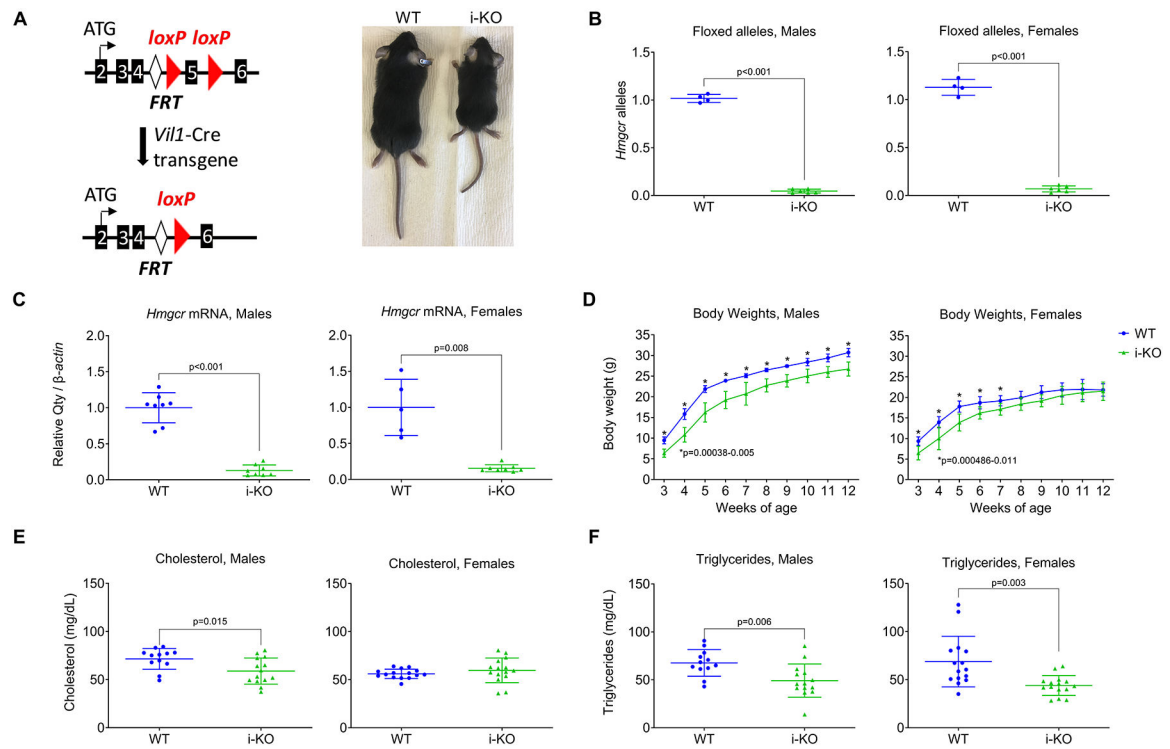


Figure 1. Generation of intestinal specific i-KO mice.

A. Conditional mice with loxP sites flanking exon 5 in the *Hmgcr* locus were generated then crossed with the *Vill1-Cre* mouse line to generate i-KO mice. A representative image of WT and i-KO mice at 4 weeks of age is on the right. **B.** Relative number of *Hmgcr* alleles as determined by ddPCR at 5 weeks of age ($n = 4$). **C.** Relative expression of *Hmgcr* mRNA determined by qPCR at 5 weeks of age ($n = 5$) in WT and i-KO mice. **D.** Body weight measurements for WT and i-KO mice from weaning through 12 weeks of age ($n = 4$). (* indicates statistical significance with p values ranging from 0.0038-0.005 in males and 0.000486-0.011 in females) **E.** Plasma cholesterol and **F.** triglyceride measurements taken at 5 weeks of age after 5 hour fast ($n = 12$). Statistical analysis was done using Welch's *t*-test, significance set at $p < 0.05$, for normally distributed data or using a Mann-Whitney test for non-normally distributed data (Triglycerides Females) and statistical significance set at $p < 0.05$. Values are mean \pm SD.

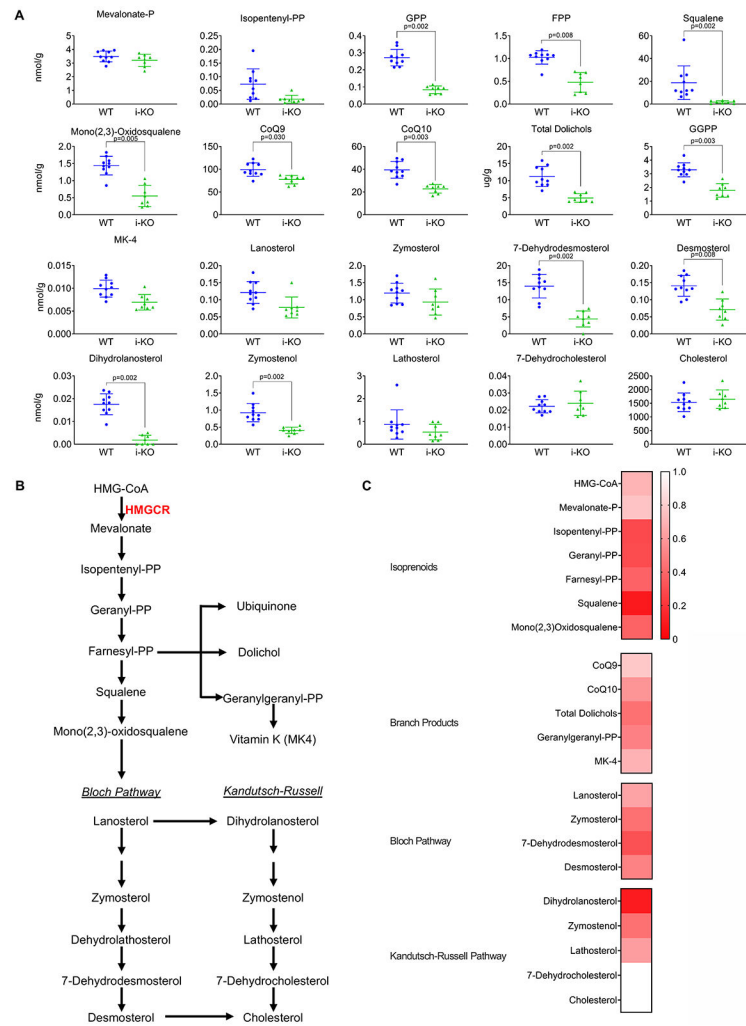


Figure 2. Targeted lipidomics reveals major reductions of sterol and non-sterol isoprenoids. **A.** Abundance of selected mevalonate-derived metabolites in epithelial scrapings derived from male mice at 5 weeks of age ($n = 8$). **B.** Abbreviated schematic of the mevalonate pathway including selected non-sterol branch products. **C.** Heat map displaying relative abundance of isoprenyl phosphates, isoprenoids and sterols. Each metabolite is compared to the mean for that metabolite in WT mice. Statistical analysis was done using the Mann-Whitney test and corrected multiple comparisons using the Holm-Šídák method (threshold for P-value comparisons, $\alpha = 0.05$). Values are mean \pm SD.

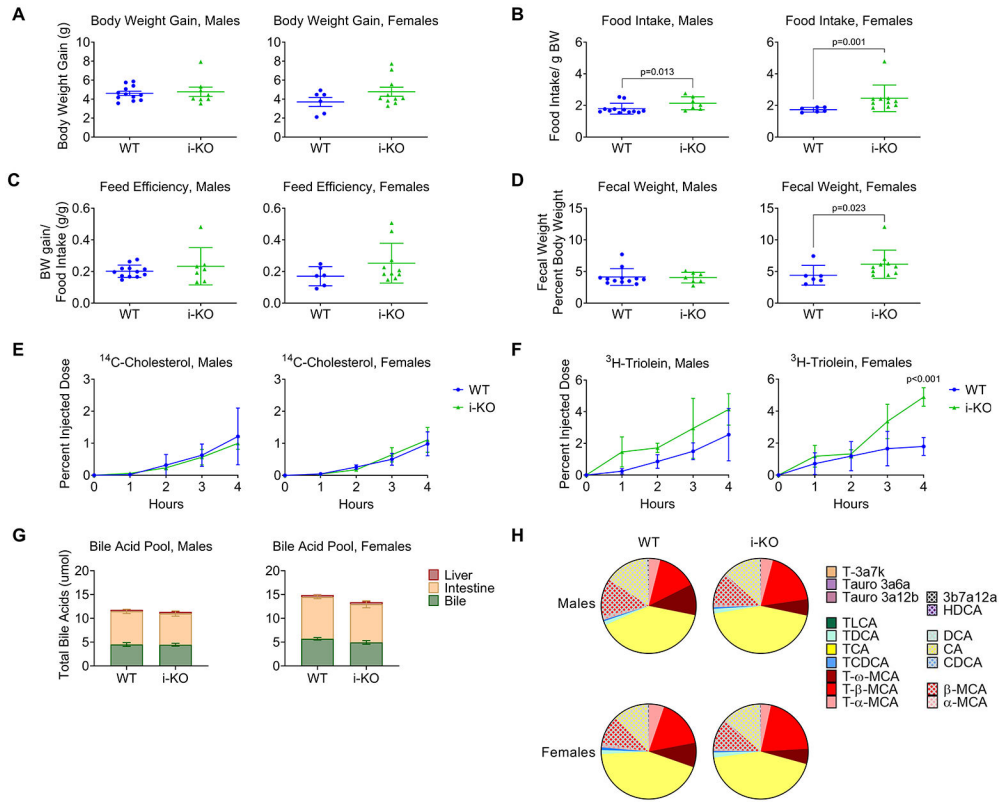


Figure 3. Food intake and feed efficiency in *Hmgcr* i-KO mice from 4 to 5 weeks of age.
A. Overall weekly body weight gain from 4 to 5 weeks of age in WT and i-KO mice ($n = 6$). **B.** Food intake in WT and i-KO mice normalized to 4-week body weight ($n = 6$). **C.** Feed efficiency in WT and i-KO mice between 4 and 5 weeks of age ($n = 6$). **D.** Total fecal weight collected over a 24-hour span as normalized to 5-week body weight beginning the day before 5 weeks of age ($n = 6$). **E.** Percent injected dose of ^{14}C -Cholesterol and **F.** ^3H -triolein in 4 week old WT and i-KO plasma over a 4-hour period after a 6-hour fast ($n=4$). **G.** The total bile acid pool and proportional contributions from liver, intestine, and bile. **H.** The total bile acid pool percent composition in WT and i-KO mice from liver, intestine, and bile. Abbreviations: HDCA, Hyodeoxycholic acid; TLCA, Tauroolithocholic acid; TDCA, Taurodeoxycholic acid; TCA, Taurocholic acid; TCDCA, Taurochenodeoxycholic acid; DCA, Deoxycholic acid; CA, Cholic acid; CDCA, Chenodeoxycholic acid; T- ω -MCA, Tauro- ω -muricholic acid; T- β -MCA, Tauro- β -muricholic acid; T- α -MCA, Tauro- α -muricholic acid; β -MCA, β -muricholic acid; α -MCA, α -muricholic acid. Statistical analysis for A through D, and at each timepoint in E and F, was done using Welch's t -test with statistical significance set at $p < 0.05$ for normally distributed data or using a Mann-Whitney test for non-normally distributed data and $p < 0.05$ (Body Weight Gain Males, Body Weight Gain Females, Food Intake Males, Food Intake Females, Feed Efficiency Males, Feed Efficiency Females, Fecal Weight Males, Fecal Weight Females). For G and H statistical analysis was done using multiple Mann-Whitney tests and corrected for multiple comparisons using the Holm-Šidák method (threshold for P-value comparisons, $\alpha = 0.05$). Values are mean \pm SD.

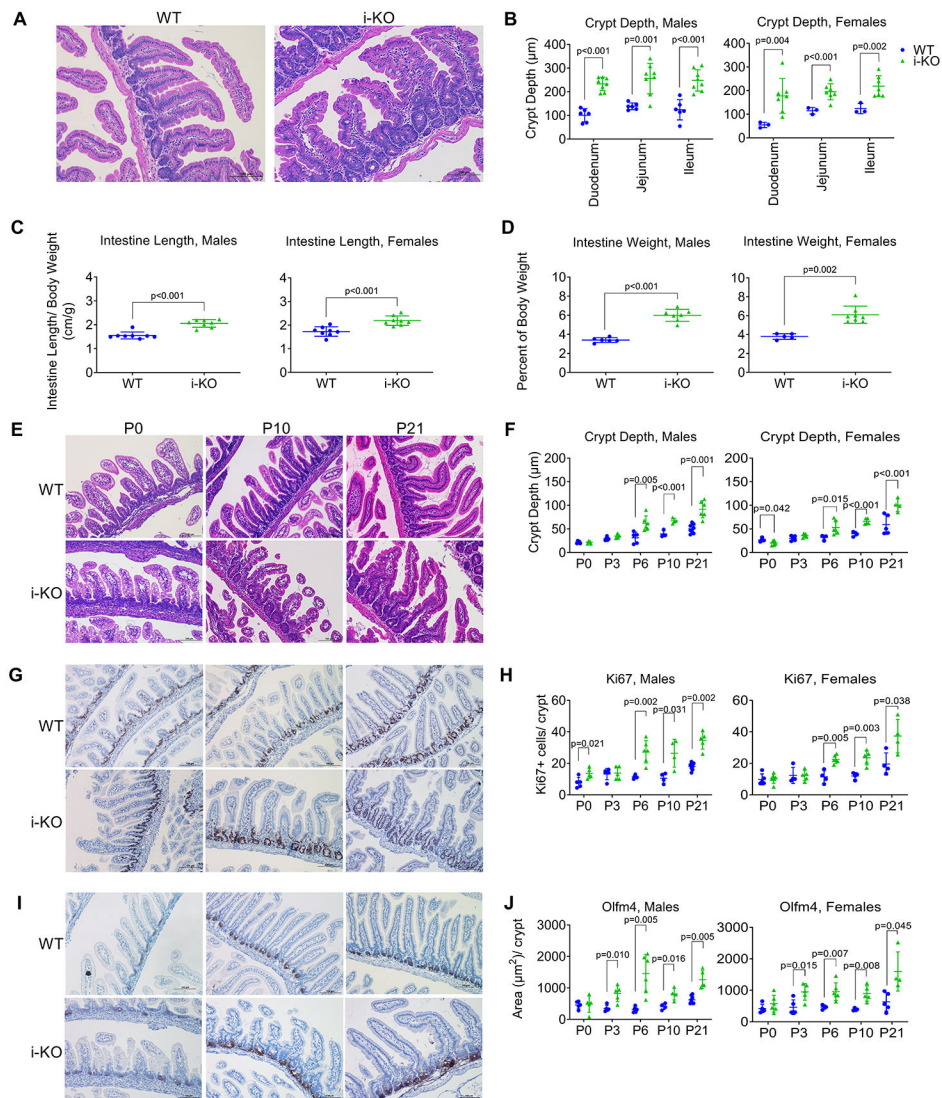


Figure 5. Time course of morphological changes in the intestine from P0 through P21.

A. Representative images of hematoxylin and eosin (H&E) staining of WT and i-KO intestines at 5 weeks of age as well as **B.** crypt depth quantification ($n = 3$). **C.** Quantification for intestine length and **D.** intestine weight normalized to body weight in i-KO and WT mice at 5 weeks of age ($n = 5$). **E.** Representative H&E images as well as **F.** crypt depth quantification for WT and i-KO at P0 through P21 ($n = 4$). **G.** Representative intestine sections stained for Ki67 and **H.** quantification of Ki67+ cells per crypt at P0 through P21 ($n = 4$). **I.** Representative intestine sections stained for Olfm4 and **J.** quantification of Olfm4+ cells per crypt at P0 through P21 ($n = 4$). Microscopy images were quantified at all time points indicated, but only representative images at P0, P10, and P21 are displayed for clarity. Scale bar is 100 μm . Statistical analysis was done using Welch's t -test and statistical significance set at $p < 0.05$ for normally distributed data or using a Mann-Whitney test for non-normally distributed data (Intestine Length Males, Intestine Weights Females) and significance set at $p < 0.05$. Values are mean \pm SD.

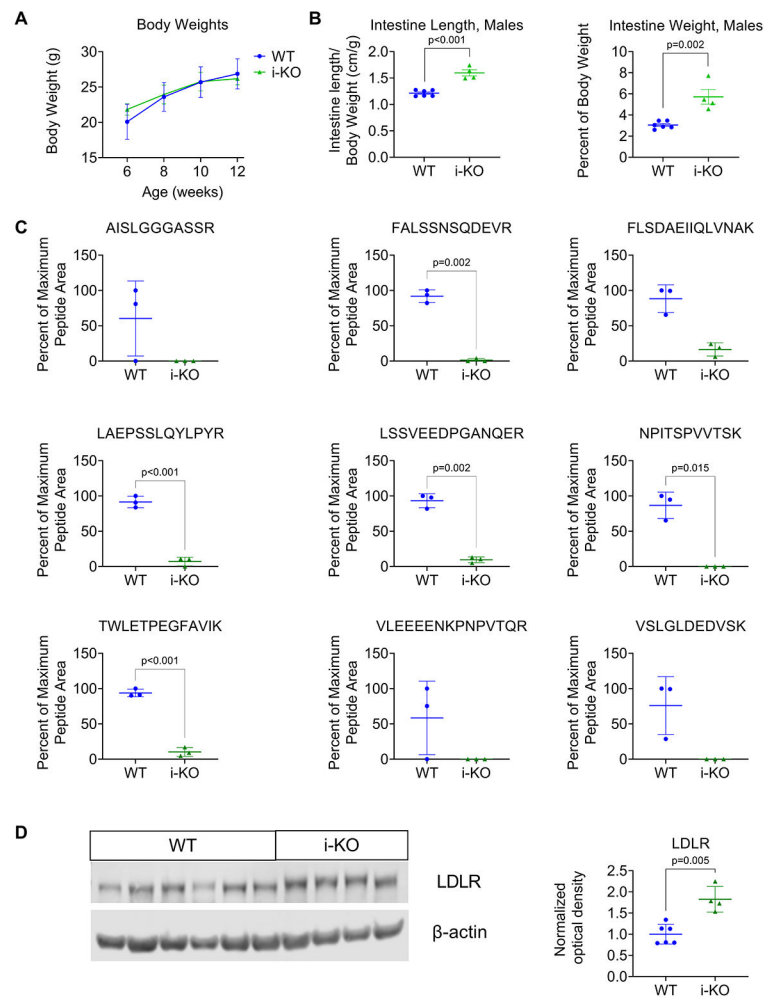


Figure 6. Analysis of male i-KO mice on 0.005% ezetimibe diet from 6 to 12 weeks of age
A. Bi-monthly body weights of mice placed on a standard laboratory diet supplemented with 0.005% ezetimibe between 6 to 12 weeks of age. **B.** Intestine length and weight of mice on ezetimibe diet at 12 weeks of age normalized to body weight. **C.** At 12 weeks of age, targeted LC-MS/MS show knockdown of 9 different HMGR peptides in i-KO mice. Note that peptide “FALSSNSQDEVR” spans a portion of the targeted exon 5. All the other peptides detected are downstream of this deleted exon. **D.** Western blot and quantification for LDLR in WT and i-KO mice on ezetimibe diet. Statistical analysis was done using Welch’s *t*-test for normally distributed data or using a Mann-Whitney test for non-normally distributed data (FLSDAEIIQLVNAK and VSLGLDEDVSK peptide analysis) with statistical significance set at $p < 0.05$. Values are mean \pm SD.